# Sheet-Type Flexible Organic Active Matrix Amplifier System Using Pseudo-CMOS Circuits With Floating-Gate Structure

Tomoyuki Yokota, Tsuyoshi Sekitani, Takeyoshi Tokuhara, Naoya Take, Ute Zschieschang, Hagen Klauk, *Member, IEEE*, Kazuo Takimiya, Tsung-Ching Huang, *Member, IEEE*, Makoto Takamiya, *Member, IEEE*, Takayasu Sakurai, *Fellow, IEEE*, and Takao Someya, *Member, IEEE*

***Abstract*—We successfully fabricated a large-area flexible strain-sensing system based on a 2-D array of organic self-bias-feedback amplifier with a signal gain of 400. The amplifier system consists of three layers: a self-assembled monolayer (SAM) capacitor matrix, a 2-D array of organic pseudo-CMOS inverters with a floating-gate structure using SAM gate dielectric, and an active matrix of organic thin-film transistors. The amplifier sheet comprises 8 $\times$ 8 amplifier cells, with an effective size of 7 $\times$ 7 $cm^2$. The organic transistors exhibit a mobility of 1.7 $cm^2/V \cdot s$ in the saturation regime at an operation voltage of 2 V. A strain sensor is made of a polymeric piezoelectric [polyvinylidene difluoride (PVDF)] sheet. When a cell of the PVDF sheet is touched (that is, when mechanical pressure is applied), a small signal is generated by intermolecular polarization in the PVDF. These signals are amplified by the organic amplifier circuits from 10 to 150 mV.**

***Index Terms*—Flexible electronics, large-area sensor, thin-film transistors (TFTs).**

## I. Introduction

Organic thin-film transistors (TFTs) [1]–[5] are expected to be used to develop a new class of electronic devices because of their mechanical flexibility and compatibility with printing processes. In the last decade, these advantages have been exploited in many types of new applications, particularly in applications such as flexible and stretchable displays [6]–[8] and RF identification tags [9]–[11]. In addition, large-area flexible sensors for detecting the spatial distribution of pressure [12], [13], temperature [14], photointensity [15], location [16], and chemical [17] and biological [18] compounds have been reported. However, the sensors developed thus far can only detect voltage signals higher than 100 mV because organic transistors have large instability and/or large variations in electronic performance.

Recently, some flexible smart organic amplifier systems have been reported [19], [20]. Marien *et al.* reported a differential amplifier with a back-gate structure. These systems amplify a signal by approximately 20 times through multiple-stage connections [19]. Ishida *et al.* reported a differential amplifier with a floating-gate structure. This amplifier can amplify a signal by approximately 5 times [20]. However, these amplifier systems have high operation voltages (greater than 10 V). Furthermore, it is a big challenge to realize simultaneous achievement of reduction in operation voltage down to a few volts and increase in gain above 100.

In this paper, we report a flexible organic amplifier system by integrating an array of organic TFTs with self-assembled monolayer (SAM) gate dielectric layers and that of SAM capacitors (see Fig. 1). The proposed system comprises 8 $\times$ 8 amplifier cells, with an effective sensing area of $7 \times 7$ $cm^2$. The organic transistors exhibit a mobility of 1.7 $cm^2/V \cdot s$ and an on/off ratio of $> 10^7$. The organic inverters adopt a pseudo-CMOS [22], [23] layout with a floating-gate structure and have a large signal gain of 400, and their switching voltage can be controlled from 1.2 to 0.44 V by charging the floating gate. This system can amplify 10-mV signals into 1-V signals. In order to show the feasibility of the amplifier, we demonstrated the amplification of 10-mV signals from ferroelectric-polymer-based strain sensors to 150-mV signals.

## II. Materials and Manufacturing Process

Each self-bias-feedback organic amplifier cell comprises an access organic TFT capacitor and a pseudo-CMOS inverter with a floating-gate structure. The circuit diagram of the amplifier system and each cell are shown in Fig. 2. Sheets containing a capacitor array, an organic transistor active matrix, and an organic amplifier array with pseudo-CMOS inverters (see Fig. 3) are separately manufactured and electrically laminated over each other. One side of a polyvinylidene difluoride (PVDF) sheet is connected to the capacitor sheet to fabricate a touch sensor system. The fabrication of each layer will be described in detail as follows.

Manuscript received July 22, 2012; revised September 3, 2012; accepted September 18, 2012. Date of current version November 16, 2012. The work of T. Yokota was supported by The Japan Society for the Promotion of Science (JSAP) Research Fellowships for Young Scientists. The review of this paper was arranged by Editor H. S. Tae.

T. Yokota is with the Department of Applied Physics, The University of Tokyo, Tokyo 113-8656, Japan (e-mail: someya@ee.t.u-tokyo.ac.jp).

T. Sekitani and T. Someya are with the Department of Electrical Engineering, The University of Tokyo, Tokyo 113-8656, Japan, and also with the Exploratory Research for Advanced Technology (ERATO), Japan Science and Technology Agency, Tokyo 113-8656, Japan.

T. Tokuhara and N. Take are with the Department of Electrical Engineering, The University of Tokyo, Tokyo 113-8656, Japan.

U. Zschieschang and H. Klauk are with the Max Planck Institute for Solid State Research, 70569 Stuttgart, Germany.

K. Takimiya is with the Department of Applied Chemistry, Graduate School of Engineering, Institute for Advanced Materials Research, Hiroshima University, Higashihiroshima 739-8527, Japan.

T.-C. Huang is with TSMC North America, San Jose, CA 95134 USA.

M. Takamiya and T. Sakurai are with the Institute of Industrial Science, The University of Tokyo, Tokyo 153-8505, Japan.

Digital Object Identifier 10.1109/TED.2012.2220853

0018-9383/$31.00 © 2012 IEEE

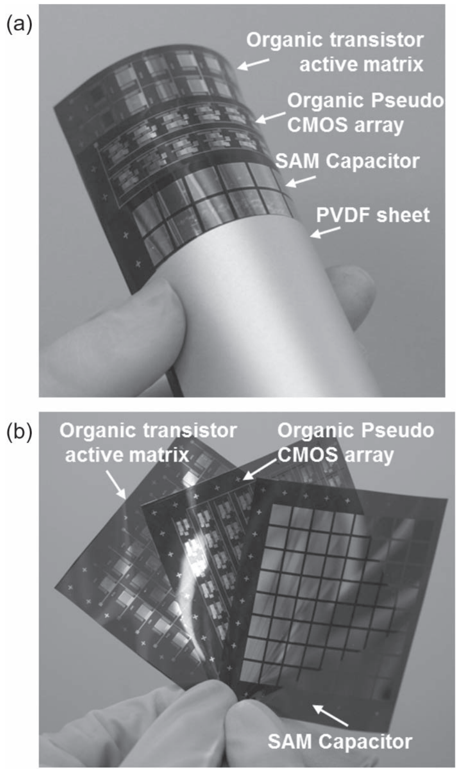


Fig. 1. Photograph of a sheet-type organic active matrix amplifier system. This system was successfully manufactured on a plastic film by integrating an active matrix of organic transistors with organic pseudo-CMOS circuits and capacitors.

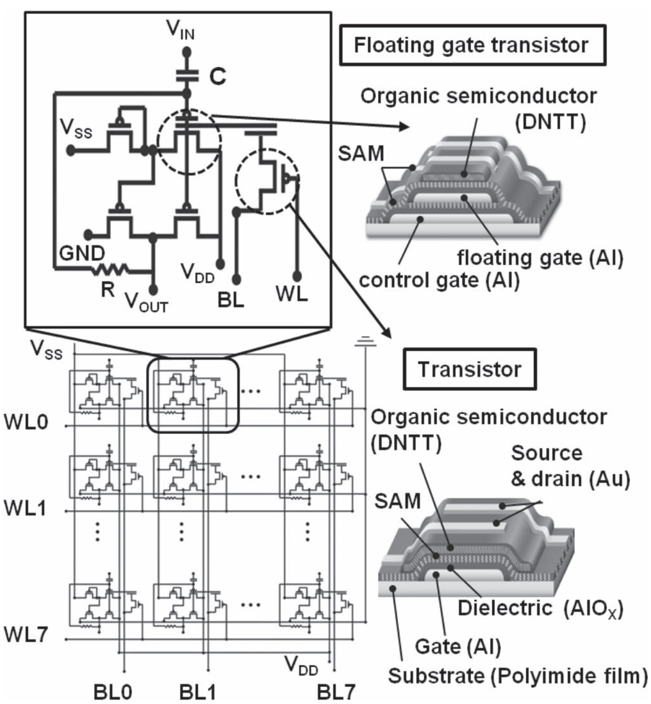


Fig. 2. Circuit diagram of an organic amplifier system. This system consists of $8 \times 8$ amplifier cells. Each amplifier cell has one capacitor, a pseudo-CMOS inverter with a floating-gate structure, and an organic transistor. Schematic cross-sectional illustrations are also shown.

## A. Organic Transistor Active Matrix

Organic transistors with top-contact geometry are fabricated on a 75-$\mu$m-thick polyimide film (UPILEX 75S, Ube

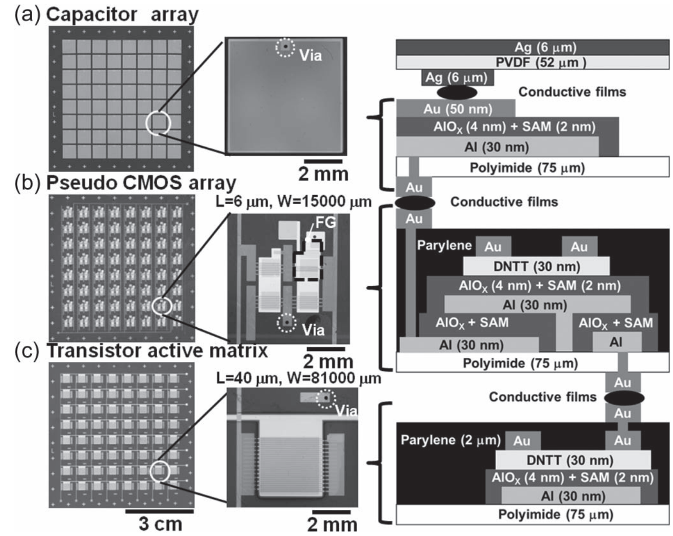


Fig. 3. Organic amplifier sheet comprising (a) capacitor array, (b) pseudo-CMOS inverter array, and (c) organic transistor active matrix. Photographs and cross-sectional images of each sheet are shown. The sheet size is 70 mm $\times$ 70 mm. These sheets are laminated using Ag paste.

Industrial). First, a 30-nm-thick aluminum (Al) layer was thermally evaporated as the gate electrode on the film substrate. As a gate dielectric layer, a 4-nm-thick aluminum oxide ($AlO_x$) layer was formed by oxygen plasma treatment and covered with a 2-nm-thick SAM by dipping into a 2-propanol solution containing 5-mM n-tetradecylphosphonic acid for 16 h at room temperature. This gate dielectric has a small leakage current and large capacitance (700 nF/cm$^2$) [24], [25]. Then, a 30-nm-thick dinaphtho[2,3-b:2′,3′-f]thieno[3,2-b]thiophene (DNTT) [26], [27] organic channel layer was deposited by vacuum evaporation using a shadow mask. Finally, a 100-nm-thick Au layer was deposited using a shadow mask to form the source and drain contacts. The manufactured transistor active matrix is encapsulated within a 2-$\mu$m-thick parylene (Daisan Kasei, Ltd., diX-SR) sheet by chemical vapor deposition. The channel length and width are 40 and 81 000 $\mu$m, respectively. The periodicity of sensor cells is 7 mm.

## B. Organic Feedback Amplifier Array Sheet

Each organic self-bias-feedback amplifier cell consists of an AlOx/SAM capacitor, an organic pseudo-CMOS inverter, and a resistor (1 M$\Omega$). The pseudo-CMOS inverters are fabricated on a 75-$\mu$m-thick polyimide film. With the exception of the floating gate, the fabrication process for the amplifier sheet is similar to that for the organic transistor active matrix. The floating gate (Al) and top dielectric ($AlO_x$/SAM) are formed by a process similar to that used for the control gate and bottom gate dielectric. The fabricated organic pseudo-CMOS inverters have a channel length of 6 $\mu$m and a channel width of 15 000 $\mu$m.

## C. PVDF Sheet

A 52-$\mu$m-thick piezoelectric PVDF film was used to make strain sensors. The surface of PVDF films was coated with Ag.

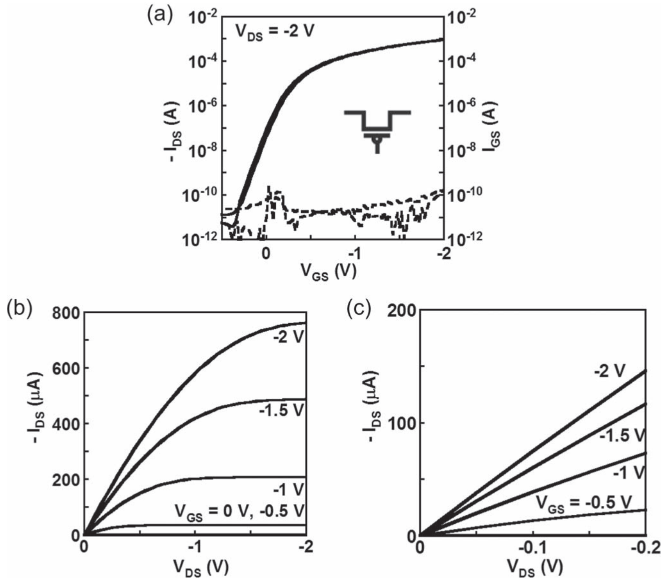


Fig. 4. Electrical characteristics of DNTT organic transistor. (a) Transfer characteristics of organic TFT with channel length and width of 15 and 6000 $\mu$m, respectively. (b) Output characteristics of organic TFT. (c) Operation of the organic field-effect transistors with a small $V_{\mathrm{DS}}$ value. A plot of $I_{\mathrm{DS}}$ versus $V_{\mathrm{DS}}$ in the linear regime.

PVDF is a ferroelectric polymer, exhibiting efficient piezoelectric and pyroelectric properties. Although the piezoelectricity of PVDF is lower than that of lead zirconate titanate (PZT), PVDF has many advantages with respect to its application to flexible electronics, such as mechanical flexibility, low weight, low cost, and compatibility with large-area manufacturing and a sheet-type morphology. These sheets are laminated using Ag conductive paste.

## III. Device Characteristics

### A. Stand-Alone Organic Transistors

Stand-alone organic transistors were characterized. We measured all transistor characteristics in air. The transistor is operated at $-2$ V because of the very thin gate dielectric layers comprising 6-nm-thick $\mathrm{AlO}_x/\mathrm{SAM}$ sheets. The typical transfer and output characteristics of the manufactured transistors are shown in Fig. 4. The mobility in the saturation regime is 1.7 $\mathrm{cm}^2/\mathrm{V}\cdot\mathrm{s}$, and the threshold voltage $(V_{\mathrm{th}})$ is almost 0 V. The leakage current is less than 200 pA, and the on/off ratio is $10^7$. As shown in Fig. 4(c), the manufactured transistors exhibit good linear behavior in the small-signal regime, indicating that good ohmic contacts can be obtained in the manufactured organic transistors.

### B. Organic Transistor With Floating Gate

Threshold voltages $(V_{\mathrm{th}})$ of organic transistors with a floating gate can be controlled by charging/discharging carriers into the floating gate when programming/erasing voltages are applied to the control gate electrode [28], [29]. Fig. 5(a) shows the transfer characteristics of DNTT floating-gate transistors. Each transfer characteristic was measured before and after a programming voltage applied to the control gate. This programming voltage was applied before the measurement and not applied during the measurement of the transfer curves. The $V_{\mathrm{th}}$ of the floating-gate transistor is plotted as a function of the programming voltage that was applied to the control gate before the measurement, as shown in Fig. 5(b). For programming voltages between 0 and $-6$ V, $V_{\mathrm{th}}$ was varied over a wide range from 0 to $-2.4$ V.

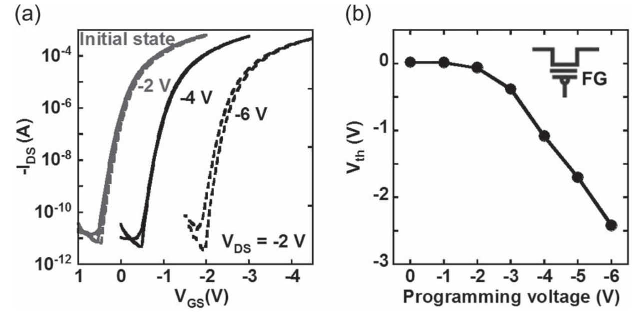


Fig. 5. Electrical characteristics of DNTT organic floating-gate transistor. (a) Transfer characteristics of the floating-gate transistors after applying a programming voltage ranging from $-1$ to $-6$ V to the control gate electrode. The duration of each program pulse was 1 s. (b) Threshold voltage as a function of programming voltage.

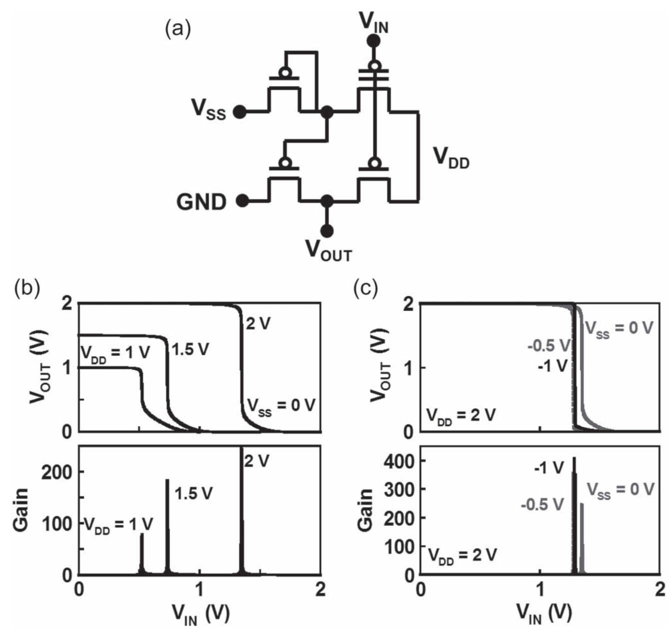


Fig. 6. Pseudo-CMOS inverter with floating gate. (a) Circuit diagram of an organic pseudo-CMOS inverter. This circuit contains only four p-type organic transistors. (b) Output voltage and signal gain as functions of driving voltage $(V_{\mathrm{DD}})$ with $V_{\mathrm{SS}}$ of 0 V. (c) Output voltage and signal gain as functions of $V_{\mathrm{SS}}$ with $V_{\mathrm{DD}}$ of 2 V.

### C. Pseudo-CMOS Inverter With Floating Gate

The characteristics of organic pseudo-CMOS inverters with a floating gate were investigated. Fig. 6(a) shows the circuit diagram of the pseudo-CMOS inverter with a floating gate. Fig. 6(b) shows the input–output characteristics of the pseudo-CMOS inverter with $V_{\mathrm{SS}} = 0$ V and a driving voltage $(V_{\mathrm{DD}})$ of 1, 1.5, and 2 V. These characteristics were measured before applying any programming voltages that exceed the inverter input voltage. The inverter exhibits a small-signal gain of

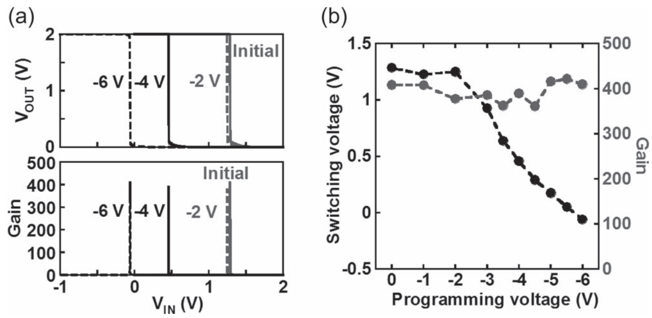


Fig. 7. Control of the switching voltage of a pseudo-CMOS inverter by applying a programming voltage to the control gate. (a) Transfer characteristics after applying a programming voltage ranging from $-1$ to $-6$ V. (b) Switching voltage as a function of programming voltage. The switching voltage is systematically shifted from 1.29 to $-0.06$ V, and the signal gain is almost constant (approximately 400).

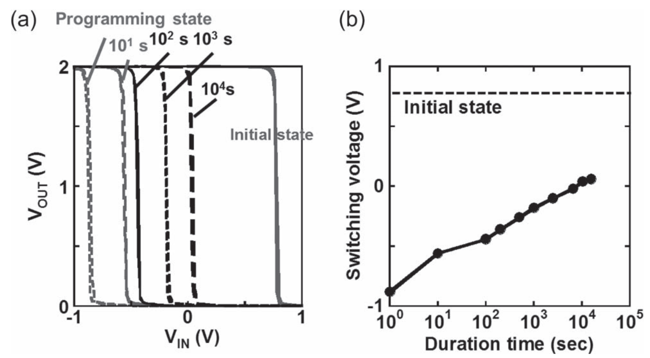


Fig. 8. Retention characteristics of the switching voltage control of the pseudo-CMOS inverter circuits. (a) Transfer characteristics of a pseudo-CMOS inverter after application of a programming voltage of $-6$ V for 1 s. The switching voltage gradually recovers its initial state. After $10^4$ s, the switching voltage is 0.04 V. (b) Switching voltage as a function of time.

approximately 100 at a supply voltage of 1 V. Fig. 6(c) shows the input–output characteristics of the pseudo-CMOS inverter for $V_{\rm SS} = 0$, $-0.5$, and $-1$ V and $V_{\rm DD} = 2$ V. The signal gain is greater than 400 for $V_{\rm SS} = -1$ V and $V_{\rm DD} = 2$ V.

Fig. 7 shows the input–output characteristics of the same pseudo-CMOS inverter for $V_{\rm DD} = 2$ V after a programming voltage was applied to the control gate. As shown, the application of a negative programming voltage caused the switching voltage of the inverter to systematically shift toward more negative voltages. This way, we can control the switching voltage by applying a programming voltage without decreasing the signal gain. The switching voltage is shifted from 1.29 to $-0.06$ V.

The retention characteristics of the pseudo-CMOS inverter with a floating gate after applying a programming voltage of $-6$ V for 1 s are shown in Fig. 8. The switching voltage gradually recovers to the initial state. After 4 h, the switching voltage shift is 0.7 V.

Fig. 9 shows that the total variation in the switching voltages of ten pseudo-CMOS inverters is approximately 400 mV before the application of a programming voltage. By applying an appropriate programming voltage, we can reduce the variation in the switching voltages to 20 mV. This result indicates that a floating-gate structure is very effective in reducing device variation.

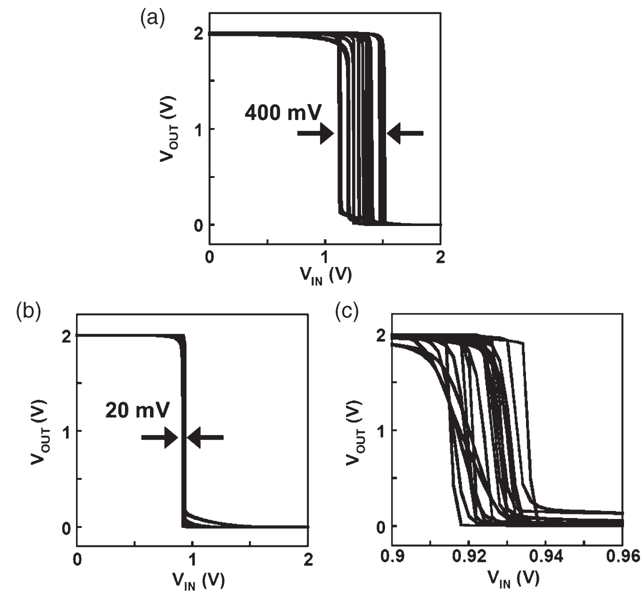


Fig. 9. Reduction in performance variation of ten pseudo-CMOS inverters with floating gates. (a) Input–output characteristics of pseudo-CMOS inverters before programming. Before applying a programming voltage to the control gate electrode, the variation of the switching voltage is approximately 400 mV. (b) Input–output characteristics of pseudo-CMOS inverters after programming. After applying an appropriate programming voltage to the control gates of each inverter, the variation in the switching voltage is reduced from 400 to 20 mV. (c) The magnification of input–output characteristics of pseudo-CMOS inverters after programming.

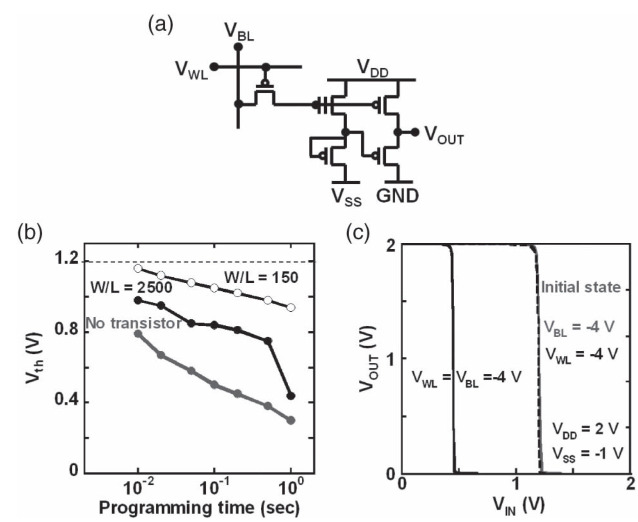


Fig. 10. Switching voltage control by using organic transistor. (a) Circuit diagram. An organic transistor is connected to the control gate of a pseudo-CMOS inverter circuit. (b) Switching voltage as a function of programming time ($V_{\rm WL} = -4$ V; $V_{\rm BL} = -4$ V). The gray circles represent the switching voltage (without transistor). The black and white circles represent a W/L ratio of 2500 and 150, respectively. (c) Output characteristics after programming by using the organic transistor with a W/L of 2500. The switching voltage of individual pseudo-CMOS inverters can be controlled by the active transistor matrix.

In a large active matrix, it is very difficult to control the switching voltage of individual pseudo-CMOS inverters in each cell. Hence, we controlled the switching voltage by using a transistor active matrix. Fig. 10(a) shows the circuit diagram. When using a transistor with a large width-to-length ratio (W/L) of 2500, the switching voltage is shifted from 1.2 to 0.44 V

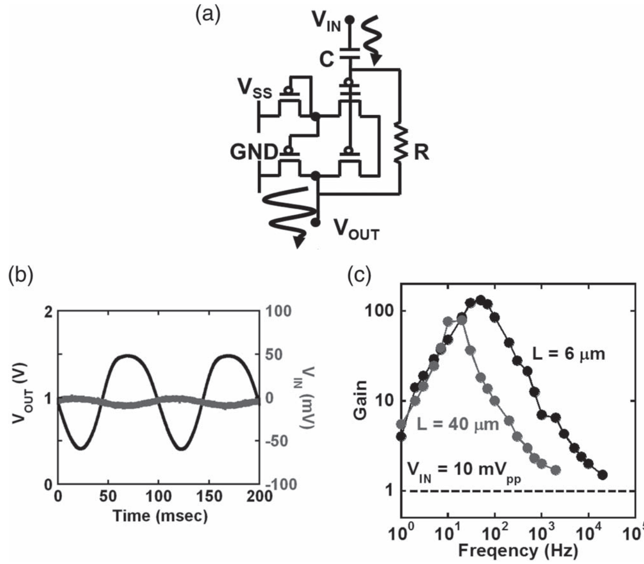


Fig. 11. Characteristics of organic pseudo-CMOS amplifier circuits. (a) Circuit diagram of organic amplifier circuit. This amplifier circuit comprises one capacitor, a pseudo-CMOS inverter, and a resistor. (b) Input and output signals. A 10-Hz sine wave is amplified from 10 to 1 $V_{PP}$. (c) Gain as a function of input frequency. Amplifier circuits with a channel length of 6 $\mu$m exhibit better frequency response than those with a channel length of 40 $\mu$m.

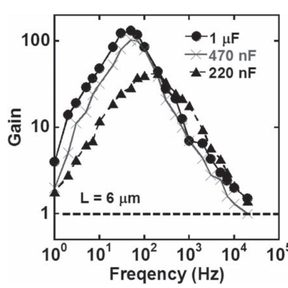


Fig. 12. Capacitance dependence of organic amplifier characteristics. The capacitance was changed from 220 nF to 1 $\mu$F. The characteristics shift to higher frequency with a decrease in the capacitance.

when the programmed $V_{\mathrm{WL}}$ and $V_{\mathrm{BL}}$ values are $-4$ V for 1 s [see Fig. 10(b)]. Then, we checked the crosstalk. When the programmed $V_{\mathrm{WL}}$ or $V_{\mathrm{BL}}$ is $-4$ V for 1 s, the switching voltage is not changed [see Fig. 10(c)]. This means that we can control the switching voltage of individual pseudo-CMOS inverters.

### *D. Feedback Amplifier Circuit*

The feedback amplifier circuits are composed of an SAM capacitor, a pseudo-CMOS inverter, and a resistor [see Fig. 11(a)]. Fig. 11(b) shows the input and output signal voltages. The gain was measured as a function of the input frequency [see Fig. 11(c)]. Black and gray dots represent amplifier circuits with a channel length of 6 and 40 $\mu$m, respectively. The frequency response at a channel length of 6 $\mu$m is approximately 10 times better than that at 40 $\mu$m. When the input signal voltage $(V_{\mathrm{IN}})$ is 10 $\mathrm{mV_{pp}}$, the maximum gain is 130 at 50 Hz, and the gain is 10 at 1 kHz.

Fig. 12 shows the capacitance dependence of the amplifier characteristics. Using a smaller capacitance, we find that the characteristics shift to higher frequencies.

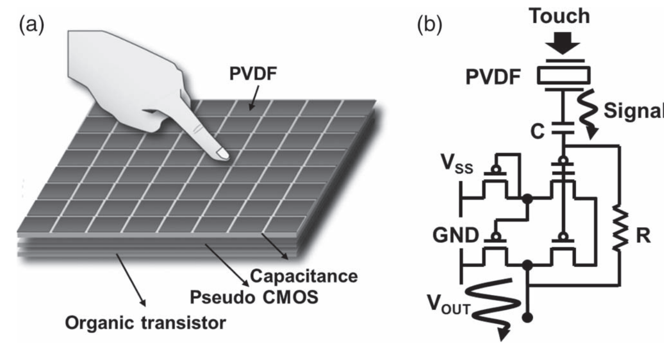


Fig. 13. Demonstration of the amplification of small signals. (a) Setup of strain-sensing sensor matrix (pressure sensor). The PVDF pressure sensor sheet and amplifier sheet are integrated. (b) Circuit diagram of strain-sensing sensor matrix. When we touch a cell of the PVDF sheet, a small signal is generated by intermolecular polarization in the PVDF. This signal is amplified by the organic amplifier circuits.

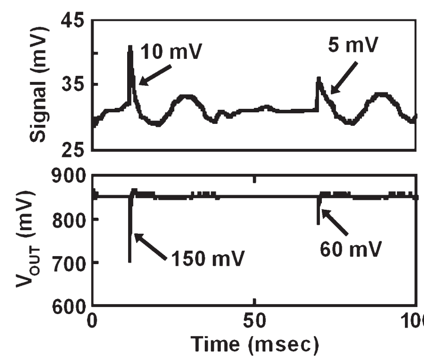


Fig. 14. Output signal before amplification and output signal $(V_{\mathrm{OUT}})$ after amplification. The small signal from intermolecular polarization is amplified from 10 and 5 mV to 150 and 60 mV, respectively.

## IV. DEMONSTRATION

The touch sensor sheet consists of an organic amplifier sheet and a PVDF sheet (see Fig. 13). When a cell of the PVDF sheet is touched (that is, mechanical pressure is applied), a small signal of approximately 10 mV is generated by intermolecular polarization in the PVDF. These signals are amplified by the organic amplifier circuits. We demonstrated amplification of the small piezoelectric signal from the flexible PVDF-based touch sensor sheet from 10 to 150 mV (see Fig. 14).

## V. DISCUSSION

We would like to address the advantages of this amplifier system. First, this amplifier system has a good frequency response and a large signal gain. Conventional organic CMOS inverters consist of p- and n-type organic transistors. Although the mobility of p-type organic transistors on SAM gate dielectric layers is higher than 2 $\mathrm{cm^2/V \cdot s}$, that for n-type organic transistors on an SAM is typically less than 0.05 $\mathrm{cm^2/V \cdot s}$ [27]. For this reason, the device speed of conventional CMOS circuits is decided by the speed of the n-type organic transistors. In contrast, conventional organic pMOS inverters exhibit high-speed response [30]. However, the signal gain of a conventional pMOS inverter is very small [30]. The pseudo-CMOS inverter is a new circuit with a large signal gain and good frequency response [23]. Pseudo-CMOS inverters comprise only four p-type organic transistors with very high mobility. Thus, we can obtain a high gain and a wide frequency response using a pseudo-CMOS inverter.

Second, we can reduce device variation by using the floating gate. In a previous study, several approaches were used to control the threshold voltage of organic TFTs, for example, surface modification of the gate dielectric [31]–[33] and surface modification of the contact metals [34]. In these methods, the threshold voltage of the transistors can be set to a specific value during manufacturing. However, it is very important to control the threshold voltage after manufacturing for reducing the device variation. One method of threshold voltage control after manufacturing involves the use of a double-gate structure [35], [36]. In this case, the control voltage must be continuously applied during operation. In contrast, in the floating-gate structure [28], [29] described here, the desired threshold voltage is programmed into the floating gate in a nonvolatile manner; therefore, the control voltage needs to be applied only briefly before circuit operation. Moreover, the floating-gate TFTs can be fabricated with very thin SAM-based dielectrics, facilitating low operating and programming voltages (2 and 6 V, respectively).

Third, this organic amplifier system has mechanical flexibility and is lightweight; thereby, it is expected to open up a new class of electronics having large-area, flexible, and cost-effective features.

Next, we discuss the frequency response of the manufactured amplifier system. In the low-frequency region, the gain increases with the signal frequency [see Fig. 11(c)]. This is because low-frequency signals are blocked by the capacitor (see Fig. 12). However, in the high-frequency region, the gain decreases with an increase in the signal frequency. A channel length of 6 $\mu$m is better than a channel length of 40 $\mu$m for the pseudo-CMOS amplifier [see Fig. 11(c)]. This means that the frequency response in the high-frequency region is limited by the speed of the pseudo-CMOS inverter. Thus, the frequency response of this amplifier system can be improved by reducing the channel length further [37]–[39] and/or improving mobility.

Although feasibility of a single cell has been proved in this work, a measurement of spatial distributions of pressure requires high yields. Indeed, our device does not exhibit 100% yield. Yields of the transistors and the capacitor are 98% and 67%, respectively. The yields are expected to be increased by reducing the device size and/or using the thicker $AlO_x$ gate dielectric layer forming by anodization method.

## VI. Summary

In this paper, we successfully fabricated a flexible organic self-bias-feedback amplifier system by integrating an SAM capacitor sheet, an array of 2-V operational organic pseudo-CMOS inverters with floating gates and a large signal gain of 400, and an active matrix of organic transistors. The switching voltages of the pseudo-CMOS inverters with floating gates can be made uniform by the randomly accessible active matrix. The system comprises 8 $\times$ 8 cells and has a work area of 7 $\times$ 7 cm$^2$. The organic active matrix feedback amplifier can amplify 10-mV signals into 1-V signals and can compensate for the instability and variations in performance. In order to show the feasibility of the amplifier, amplification of 10-mV signals from ferroelectric-polymer-based strain sensors into 150-mV signals was demonstrated.

## Acknowledgment

The authors would like to thank Nippon Kayaku Co., Ltd. for providing high-purity DNTT.

## References

[1] S. R. Forrest, “The path to ubiquitous and low-cost organic electronic appliances on plastic,” *Nature*, vol. 428, no. 6986, pp. 911–918, Apr. 2004.

[2] G. Horowitz, “Organic thin film transistors: From theory to real devices,” *J. Mater. Res.*, vol. 19, no. 7, pp. 1946–1962, Jul. 2004.

[3] H. Sirringhaus, “Device physics of solution-processed organic field-effect transistors,” *Adv. Mater.*, vol. 17, no. 20, pp. 2411–2425, Oct. 2005.

[4] H. Klauk, *Organic Electronics: Materials, Manufacturing, and Applications*. Weinheim, Germany: Wiley, Aug. 2006.

[5] Z. Bao and J. Locklin, *Organic Field-Effect Transistors*. Boca Raton, FL: CRC Press, May 2007.

[6] J. A. Rogers, Z. Bao, K. Baldwin, A. Dodabalapur, B. Crone, V. R. Raju, V. Kuck, H. Katz, K. Amundson, J. Ewing, and P. Drzaic, “Paperlike electronic displays: Large-area rubberstamped plastic sheets of electronics and microencapsulated electrophoretic inks,” *Proc. Nat. Acad. Sci.*, vol. 98, no. 9, pp. 4835–4840, Apr. 2001.

[7] G. H. Gelinck, H. E. A. Huitema, E. Van Veenendaal, E. Cantatore, L. Schrijnemakers, J. B. P. H. Van der Putten, T. C. T. Geuns, M. Beenhakkers, J. B. Giesbers, B. H. Huisman, E. J. Meijer, E. M. Benito, F. J. Touwslager, A. W. Marsman, B. J. E. Van Rens, and D. M. De Leeuw, “Flexible active-matrix displays and shift registers based on solution-processed organic transistors,” *Nat. Mater.*, vol. 3, no. 2, pp. 106–110, Feb. 2004.

[8] K. Nomoto, N. Hirai, N. Yoneya, N. Kawashima, M. Noda, M. Wada, and J. Kasahara, “A high-performance short-channel bottom-contact OTFT and its application to AM-TN-LCD,” *IEEE Trans. Electron Devices*, vol. 52, no. 7, pp. 1519–1526, Jul. 2005.

[9] P. F. Baude, D. A. Ender, M. A. Haase, T. W. Kelley, D. V. Muyres, and S. D. Theiss, “Pentacene-based radio-frequency identification circuitry,” *Appl. Phys. Lett.*, vol. 82, no. 22, pp. 3964–3966, Jun. 2003.

[10] V. Subramanian, P. C. Chang, and J. B. Lee, “Printed organic transistors for ultra-low-cost RFID applications,” *IEEE Trans. Compon. Packag. Technol.*, vol. 28, no. 4, pp. 742–747, Dec. 2005.

[11] S. Steudel, K. Myny, V. Arkhipov, C. Deibel, and P. Heremans, “50 MHz rectifier based on an organic diode,” *Nat. Mater.*, vol. 4, no. 8, pp. 597–600, Aug. 2005.

[12] T. Someya, T. Sekitani, S. Iba, Y. Kato, H. Kawaguchi, and T. Sakurai, “A large-area, flexible pressure sensor matrix with organic field-effect transistors for artificial skin applications,” *Proc. Nat. Acad. Sci.*, vol. 101, no. 27, pp. 9966–9970, Jul. 2004.

[13] S. C. B. Mannsfeld, B. C.-K. Tee, R. M. Stoltenberg, C. V. H.-H. Chen, S. Barman, B. V. O. Muir, A. N. Sokolov, C. Reese, and Z. Bao, “Highly sensitive flexible pressure sensors with microstructured rubber dielectric layers,” *Nat. Mater.*, vol. 9, no. 10, pp. 859–864, Oct. 2010.

[14] I. Graz, M. Krause, S. B. Gogonea, S. Bauer, S. P. Lacour, B. Ploss, M. Zirkl, B. Stadlober, and S. Wagne, “Flexible active-matrix cells with selectively poled bifunctional polymerceramic nanocomposite for pressure and temperature sensing skin,” *J. Appl. Phys.*, vol. 106, no. 3, p. 034503, Aug. 2009.

[15] T. N. Ng, W. S. Wong, M. L. Chabinyc, S. Sambandan, and R. A. Street, “Flexible image sensor array with bulk heterojunction organic photodiode,” *Appl. Phys. Lett.*, vol. 92, no. 21, p. 213 303, May 2008.

[16] G. Buchberger, R. Schwödiauer, and S. Bauer, “Flexible large area ferroelectret sensors for location sensitive touchpads,” *Appl. Phys. Lett.*, vol. 92, no. 12, p. 123 511, Mar. 2008.

[17] M. E. Roberts, S. C. B. Mannsfeld, N. Queraltó, C. Reese, J. Locklin, W. Knoll, and Z. Bao, “Water-stable organic transistors and their application in chemical and biological sensors,” *Proc. Nat. Acad. Sci.*, vol. 105, no. 34, pp. 12 134–12 139, Aug. 2008.

[18] C. Bartic and G. Borghs, "Organic thin-film transistors as transducers for (bio) analytical applications," *Anal. Bioanal. Chem.*, vol. 384, no. 2, pp. 354–365, Jan. 2006.

[19] H. Marien, M. S. J. Steyaert, E. van Veenendaal, and P. Heremans, "A fully integrated $\Delta\Sigma$ ADC in organic thin-film transistor technology on flexible plastic foil," *IEEE J. Solid-State Circuits*, vol. 46, no. 1, pp. 276–284, Jan. 2011.

[20] K. Ishida, T. C. Huang, K. Honda, T. Sekitani, H. Nakajima, H. Maeda, M. Takamiya, T. Someya, and T. Sakurai, "A 100-V AC energy meter integrating 20-V organic CMOS digital and analog circuits with a floating gate for process variation compensation and a 100-V organic pMOS rectifier," *IEEE J. Solid-State Circuits*, vol. 47, no. 1, pp. 301–309, Jan. 2012.

[21] T. Yokota, T. Sekitani, T. Tokuhara, U. Zschieschang, H. Klauk, T. C. Huang, M. Takamiya, T. Sakurai, and T. Someya, "Sheet-type organic active matrix amplifier system using Vth-tunable, pseudo-CMOS circuits with floating-gate structure," in *Proc. IEEE IEDM*, Dec. 2011, pp. 14.4.1–14.4.4.

[22] T. C. Huang, K. Fukuda, C. M. Lo, Y. H. Yeh, T. Sekitani, T. Someya, and K. T. Cheng, "Pseudo-CMOS: A design style for low-cost and robust flexible electronics," *IEEE Trans. Electron Devices*, vol. 58, no. 1, pp. 141–150, Jan. 2011.

[23] K. Fukuda, T. Sekitani, T. Yokota, K. Kuribara, T. C. Huang, T. Sakurai, U. Zschieschang, H. Klauk, M. Ikeda, H. Kuwabara, T. Yamamoto, K. Takimiya, K. T. Cheng, and T. Someya, "Organic pseudo-CMOS circuits for low-voltage large-gain high-speed operation," *IEEE Electron Device Lett.*, vol. 32, no. 10, pp. 1448–1450, Oct. 2011.

[24] H. Klauk, U. Zschieschang, J. Pflaum, and M. Halik, "Ultralow-power organic complementary circuits," *Nature*, vol. 445, no. 7129, pp. 745–748, Feb. 2007.

[25] K. Fukuda, T. Yokota, K. Kuribara, T. Sekitani, U. Zschieschang, H. Klauk, and T. Someya, "Thermal stability of organic thin-film transistors with self-assembled monolayer dielectrics," *Appl. Phys. Lett.*, vol. 96, no. 5, p. 053302, Feb. 2010.

[26] T. Yamamoto and K. Takimiya, "Facile synthesis of highly $\pi$-extended heteroarenes, dinaphtho[2,3-b:2′,3′-f]chalcogenopheno[3,2-b]chalcogenophenes, and their application to field-effect transistors," *J. Amer. Chem. Soc.*, vol. 129, no. 8, pp. 2224–2225, Feb. 2007.

[27] U. Zschieschang, F. Ante, T. Yamamoto, K. Takimiya, H. Kuwabara, M. Ikeda, T. Sekitani, T. Someya, K. Kern, and H. Klauk, "Flexible low-voltage organic transistors and circuits based on a high-mobility organic semiconductor with good air stability," *Adv. Mater.*, vol. 22, no. 9, pp. 982–985, Mar. 2010.

[28] T. Sekitani, T. Yokota, U. Zschieschang, H. Klauk, S. Bauer, K. Takeuchi, M. Takamiya, T. Sakurai, and T. Someya, "Organic nonvolatile memory transistors for flexible sensor arrays," *Science*, vol. 326, no. 5959, pp. 1516–1519, Dec. 2009.

[29] T. Yokota, T. Nakagawa, T. Sekitani, Y. Noguchi, K. Fukuda, U. Zschieschang, H. Klauk, K. Takeuchi, M. Takamiya, T. Sakurai, and T. Someya, "Control of threshold voltage in low-voltage organic complementary inverter circuits with floating gate structures," *Appl. Phys. Lett.*, vol. 98, no. 19, p. 193 302, May 2011.

[30] U. Zschieschang, F. Ante, D. Kälblein, T. Yamamoto, K. Takimiya, H. Kuwabara, M. Ikeda, T. Sekitani, T. Someya, J. Blochwitz-Nimoth, and H. Klauk, "Dinaphtho[2,3-b:2′,3′-f]thieno[3,2-b]thiophene (DNTT) thin-film transistors with improved performance and stability," *Organ. Electron.*, vol. 12, no. 8, pp. 1370–1375, Aug. 2011.

[31] S. Kobayashi, T. Nishikawa, T. Takenobu, S. Mori, T. Shimoda, T. Mitani, H. Shimotani, N. Yoshimoto, S. Ogawa, and Y. Iwasa, "Control of carrier density by self-assembled monolayers in organic field-effect transistors," *Nat. Mater.*, vol. 3, no. 5, pp. 317–322, May 2004.

[32] P. Pernstich, S. Haas, D. Oberhoff, C. Goldmann, D. J. Gundlach, B. Batlogg, A. N. Rashid, and G. Schitter, "Threshold voltage shift in organic field effect transistors by dipole monolayers on the gate insulator," *J. Appl. Phys.*, vol. 96, no. 11, pp. 6431–6438, Dec. 2004.

[33] U. Zschieschang, F. Ante, M. Schlörholz, M. Schmidt, K. Kern, and H. Klauk, "Mixed self-assembled monolayer gate dielectrics for continuous threshold voltage control in organic transistors and circuits," *Adv. Mater.*, vol. 22, no. 40, pp. 4489–4493, Oct. 2010.

[34] M. Kitamura, Y. Kuzumoto, S. Aomori, M. Kamura, J. H. Na, and Y. Arakawa, "Threshold voltage control of bottom-contact n-channel organic thin-film transistors using modified drain/source electrodes," *Appl. Phys. Lett.*, vol. 94, no. 8, p. 083310, Feb. 2009.

[35] K. Hizu, T. Sekitani, T. Someya, and J. Otsuki, "Reduction in operation voltage of complementary organic thin-film transistor inverter circuits using double-gate structures," *Appl. Phys. Lett.*, vol. 90, no. 9, p. 093504, Feb. 2007.

[36] K. Myny, E. van Veenendaal, G. H. Gelinck, J. Genoe, W. Dehaene, and P. Heremans, "An 8-bit, 40-instructions-per-second organic microprocessor on plastic foil," *IEEE J. Solid-State Circuits*, vol. 47, no. 1, pp. 284–291, Jan. 2012.

[37] K. Murata, "Super-fine ink-jet printing for nanotechnology," in *Proc. ICMENS*, Jul. 2003, pp. 346–349.

[38] T. Sekitani, Y. Noguchi, U. Zschieschang, H. Klauk, and T. Someya, "Organic transistors manufactured using inkjet technology with subfemtoliter accuracy," *Proc. Nat. Acad. Sci.*, vol. 105, no. 13, pp. 4976–4980, Apr. 2008.

[39] T. Yokota, T. Sekitani, Y. Kato, K. Kuribara, U. Zschieschang, H. Klauk, T. Yamamoto, K. Takimiya, H. Kuwabara, M. Ikeda, and T. Someya, "Low-voltage organic transistor with subfemtoliter inkjet source–drain contacts," *MRS Commun.*, vol. 1, no. 1, pp. 3–6, Nov. 2011.


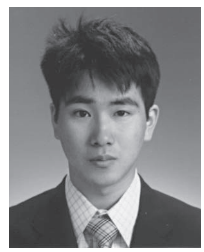

**Tomoyuki Yokota** received the M.S. degree in applied physics from The University of Tokyo, Tokyo, Japan, in 2010. He is currently working toward the Ph.D. degree in applied physics at The University of Tokyo.

**Tsuyoshi Sekitani** received the Ph.D. degree in applied physics from The University of Tokyo, Tokyo, Japan, in 2003.

In 2011, he was made an Associate Professor in the School of Engineering, The University of Tokyo.

**Takeyoshi Tokuhara** received the B.S. degree in electrical engineering from The University of Tokyo, Tokyo, Japan, in 2011. He is currently working toward the M.S. degree in electrical engineering at The University of Tokyo.

**Naoya Take** received the B.S. degree in electrical engineering from The University of Tokyo, Tokyo, Japan, in 2012. He is currently working toward the M.S. degree in electrical engineering at The University of Tokyo.

**Ute Zschieschang** received the Ph.D. degree in chemistry from TU Bergakademie Freiberg, Germany, in 2006.

Since 2005, she has been a Scientist with the Organic Electronics Group, Max Planck Institute for Solid State Research, Stuttgart, Germany.

**Hagen Klauk** (S'97–M'99) received the Ph.D. degree in electrical engineering from Pennsylvania State University, University Park, in 1999.

Since 2005, he has been Head of the Organic Electronics Group, Max Planck Institute for Solid State Research, Stuttgart, Germany.

**Kazuo Takimiya** received the Ph.D. degree from Hiroshima University, Higashihiroshima, Japan, in 1994, under the supervision of Prof. F. Ogura.

Since 2007, he has been a Full Professor with Hiroshima University.

**Tsung-Ching Huang** (S'05–M'09) received the Ph.D. degree in electrical and computer engineering from the University of California, Santa Barbara, in 2009.

He is currently a Senior Design Engineer with TSMC North America, San Jose, CA.

**Makoto Takamiya** (S'98–M'00) received the B.S., M.S., and Ph.D. degrees in electronic engineering from The University of Tokyo, Tokyo, Japan, in 1995, 1997, and 2000, respectively.

He is currently an Associate Professor with The University of Tokyo.

**Takayasu Sakurai** (S'77–M'78–SM'01–F'03) received the Ph.D. degree in electronic engineering from The University of Tokyo, Tokyo, Japan, in 1981.

Since 1996, he has been a Professor with The University of Tokyo.

**Takao Someya** (M'03) received the Ph.D. degree in electrical engineering from The University of Tokyo, Tokyo, Japan, in 1997.

Since 2009, he has been a Professor of electrical and electronic engineering with The University of Tokyo.